ACS APPLIED MATERIALS & INTERFACES

Research Article

www.acsami.org

Phosphonate- and Carboxylate-Based Self-Assembled Monolayers for Organic Devices: A Theoretical Study of Surface Binding on Aluminum Oxide with Experimental Support

Thilo Bauer,[†] Thomas Schmaltz,[‡] Thomas Lenz,[‡] Marcus Halik,[‡] Bernd Meyer,[†] and Timothy Clark*[,†]

[†]Computer-Chemistry-Center and Interdisciplinary Center for Molecular Materials, Department of Chemistry and Pharmacy, Friedrich-Alexander-Universität Erlangen-Nürnberg, Nägelsbachstrasse 25, 91052 Erlangen, Germany

[‡]Organic Materials and Devices, Institute of Polymer Materials, Department of Materials Science, Friedrich-Alexander-Universität Erlangen-Nürnberg, Martensstrasse 7, 91058 Erlangen, Germany

Supporting Information

ABSTRACT: We report a computational study on the chemical bonding of phosphonates and carboxylates to aluminum oxide surfaces and how the binding properties are related to the amount of water in the experimental environment. Two different surface structures were used in the calculations in order to model representative adsorption sites for the phosphonates and carboxylates and to account for the amorphous nature of the hydroxylated AlO_x films in experiment. For the phosphonates, we find that the thermodynamically preferred binding mode changes between mono-, bi-, and tridentate depending on the surface structure and the amount of residual water. For the carboxylates, on the other hand, monodentate adsorption is always lower in energy at all experimental conditions. Phosphonates are more strongly bound to aluminum oxide than carboxylates, so that carboxylates can be replaced easily by phosphonates. The theoretical findings are consistent with those obtained in adsorption, desorption, and exchange reactions of *n*-alkyl phosphonic and carboxylic acids on AlO_x surfaces. The results provide an atomistic understanding of the adsorption and help to optimize experimental conditions for self-assembly of organic films on aluminum oxide surfaces.

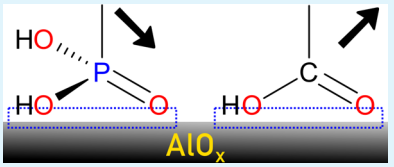

KEYWORDS: *aluminum oxide, self-assembled monolayers, phosphonates, carboxylates, exchange reaction, electronic devices*

INTRODUCTION

Self-assembled monolayers (SAMs) of organic molecules on oxidized metals or semiconductors (usually aluminum or silicon) are gaining importance as functional components of low-voltage electronic devices.[1−6] Their main advantages are that they provide excellent insulating dielectric layers despite their thinness and that the self-assembled monolayer can be fabricated by a simple dipping or printing technique.[1,7] Recently, field-effect transistors have been reported in which both the insulating dielectric and the semiconductor layer are incorporated into the molecules that make up the SAM, thus allowing the two functional layers to be produced in a single step.[8−10] Fabricating such devices requires close control of the characteristics and structure of the SAM, including producing SAMs that consist of mixtures of molecules.[11−15] In order to achieve this control, we need to understand the thermodynamics and structural aspects of binding typical SAM molecules to the oxidized surface. Several different binding modes have been proposed and discussed, but mechanistic knowledge on exchange reactions is still limited.[16] We now report a theoretical study of the binding of alkyl phosphonates and carboxylates to aluminum oxide surfaces. Functionalized phosphonates and carboxylates have been used extensively for SAMs in devices and provide two alternative types of anchor group that bind with differing strengths, so that SAMs can be tailored by, for instance, displacing carboxylates in a preformed SAM with phosphonates as shown in recent experiments. This approach was used to demonstrate a continuous shift in threshold voltage in organic transistors as a function of the different dipolar natures of the SAM molecules and their composition ratios.[17]

COMPUTATIONAL METHODS

Density-Functional Theory Calculations. Density-functional theory (DFT) calculations were performed in the generalized gradient approximation (GGA) using the Perdew-Burke-Ernzerhof (PBE) exchange-correlation functional,[18] Vanderbilt ultrasoft pseudopotentials,[19] and a plane-wave basis set expansion of the electronic wave functions with a kinetic energy cutoff of 25 Ry as implemented in the PWscf code of the Quantum Espresso software package.[20]

The aluminum oxide (0001) surfaces were represented by periodic slabs constructed from the thermodynamically most stable α-Al_2O_3 phase (corundum). In the bulk, each Al is octahedrally coordinated by six oxygen atoms, whereas all oxygens have four Al nearest neighbors. The corundum hexagonal unit cell contains six formula units of Al_2O_3. With our computational setup, we obtain bulk lattice constants of a = 4.815 Å and c = 13.142 Å, which are in very good agreement with experimental values.[21] The periodic slabs were separated by a vacuum region of about 20.2 Å perpendicular to the surface plane, and the theoretical lattice constants were used for the lateral extension of the slabs. The slab thickness was determined by calculating the surface and

Received: March 6, 2013
Accepted: June 4, 2013
Published: June 4, 2013

   dx.doi.org/10.1021/am4008374 | ACS Appl. Mater. Interfaces 2013, 5, 6073−6080

adsorption energies of water for several slabs with varying number of aluminum oxide layers. The slab consisting of three Al−O_3−Al triple-layers proved to be sufficient for obtaining well-converged results and was thus used as initial configuration for the construction of our hydroxylated model surfaces (see below). Of the three triple-layers, only the upper four atomic layers were allowed to relax, whereas the atoms in the bottom five layers were kept fixed at their bulk positions to simulate the properties of the underlying extended aluminum oxide bulk. Geometries were optimized until all components of the atomic forces were smaller than a threshold of 5 meV/Å. For slabs with a primitive (1 × 1) surface unit cell, the Brillouin zone was sampled over a 6 × 6 × 1 k-point grid. The k-point density was reduced to 3 × 3 × 1 for the slabs with a larger (2 × 2) unit cell.

The main interest of our computational study is to identify the fundamental binding mode of phosphonic and carboxylic acids on aluminum oxide in the limit of isolated molecules. Therefore, we replaced in our calculations the longer alkyl chained molecules *n*-octadecylphosphonic acid (C_{18}−PA) and stearic acid (C_{17}−CA) (see Figure 8b) used in the experiments by the simpler molecules methyl phosphonic acid and acetic acid. The molecular reference energies of isopropanol (IPA), water (W), methyl phosphonic acid (PA), and acetic acid (AA) for the calculation of adsorption energies and our thermodynamic analysis were obtained by optimizing each molecule in a cubic box with dimension of at least 13.5 Å^3.

Model Surface Structures. The thermodynamically most stable water-free α-Al_2O_3(0001) surface has a (1 × 1) periodicity and is terminated by a layer of Al atoms. Each surface Al atom is coordinated to three oxygen atoms in the subsurface layer. The surface structure is formally obtained by cutting the hexagonal unit cell perpendicular to the *c*-direction. This Al-terminated surface is found experimentally under ultrahigh-vacuum (UHV) conditions[22] and has been shown to be unexpectedly stable toward oxygen in the absence of hydrogen[23] due to the inability of Al^{3+} to oxidize further.[24] We term this structure (1 × 1)-Al and use it as reference for the calculation of formation energies of adsorbate structures on different hydroxylated aluminum oxide substrates.

In the presence of both oxygen and hydrogen, i.e., water, the surface is highly reactive because of its partially coordinated surface Al atoms and becomes hydroxylated.[23,25] This will be the case under the experimental non-UHV conditions at which the organic SAMs are prepared. To mimic representative structural motives of the hydroxylated aluminum oxide layers as they are prepared in the experiments, we considered two different water-saturated model surface structures in our calculations.

The first hydroxylated aluminum oxide model surface structure is derived by saturating the (1 × 1)-Al surface with water from air moisture to account for the experimental ambient conditions. The appropriate degree of hydroxylation was determined by placing an increasing number of water molecules in varying configurations on the surface and relaxing the structure. Because the terminal Al atoms (denoted as Al_{surf}) on (1 × 1)-Al are coordinated to only three surface oxygen atoms (O_{surf}) compared to the 6-fold coordination of Al in bulk α-Al_2O_3, we considered each Al_{surf} to be able to coordinate up to three water molecules. The water molecules were placed on the unrelaxed (1 × 1)-Al surface directly after cutting the bulk unit cell. Prior optimization of the bare surface would lead to significant structural relaxations of the surface atoms[26] which are largely reversed by the adsorbed water molecule.

The adsorption of the first water molecule on (1 × 1)-Al is strongly exothermic. The molecule dissociates spontaneously in the geometry optimization, with the hydroxyl group binding to Al_{surf} and the proton H_{diss} to one of the three oxygen atoms O_{surf} coordinated to Al_{surf}. The three O_{surf} atoms are not equivalent, but different choices of the H_{diss} binding site lead to changes in the total energy of only a few meV or less and can be neglected. The energy gain for adsorption of a second and third water molecule is much smaller. Only the second water molecule is able to coordinate to an Al_{surf}. The third water molecule is integrated into a hydrogen bonding network, and its binding energy has reached a value that corresponds to the cohesion energy in liquid water.[27] Molecular adsorption is now much more favorable. Dissociation is only observed for the first adsorbed water molecule.

In this study, we focus on the surface structure with one adsorbed water molecule per (1 × 1) surface unit cell. For the calculations of the isopropanol, methyl phosphonic acid, and acetic acid adsorption properties, the (1 × 1) slab was doubled in both directions parallel to the surface. This (2 × 2)-Al-4W configuration, which contains four dissociated water molecules, is shown in Figure 1a.

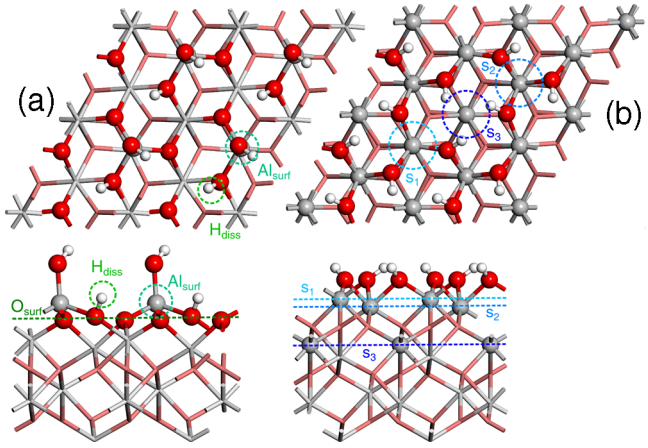

Figure 1. Top and side view of (a) the (2 × 2)-Al-4W surface and (b) the (2 × 2)-OH-6W surface together with the different binding positions $s_{1,2,3}$. Hydrogen atoms are shown in white, oxygen in red, and aluminum in gray. The same color coding is used in all other figures.

The thermodynamic ground state of the α-Al_2O_3(0001) surface under moist environmental conditions, however, is not the (2 × 2)-Al-4W structure but a reconstructed surface with a termination of a layer of hydroxyl groups.[28] This surface structure is formally obtained from (1 × 1)-Al by removing the terminal Al_{surf} and saturating the vacant surface O atoms with hydrogen.[28] The result is again a stoichiometric, oxidized surface as can be seen in the following way: first, we double the unit cell of the water-free (1 × 1)-Al surface in both directions. The top two surface layers in the (2 × 2)-Al unit cell now contain four Al and twelve O. Then, we remove two Al_2O_3 formula units, thereby creating six vacant O sites. Finally, six water molecules are dissociated. The OH groups fill the vacant O sites, and the dissociated H_{diss} adsorb on the remaining O_{surf}:

$$4(O_3Al)^{surf} + 6H_2O^{gas} \rightarrow 2(Al_2O_3)^{bulk} + 12(OH)^{surf} \quad (1)$$

This OH-terminated pseudo gibbsite (2 × 2)-OH-6W surface (see Figure 1b) is the thermodynamically most stable configuration of α-Al_2O_3(0001) in contact with water for a wide range of experimentally accessible water chemical potentials (see Supporting Information). This structure was therefore used in previous theoretical studies of phosphonic acid adsorption on aluminum oxide.[29,30] However, for the formation of the reconstructed (2 × 2)-OH-6W surface structure, the kinetic hindrance caused by the movement of two Al_2O_3 units is not easily overcome. Such drastic reconstruction of the surface has not been observed under conditions of low humidity, and an Al-terminated hydroxylated surface is believed to be the favored configuration in this case.[28] In our calculations, we therefore considered both structures, (2 × 2)-Al-4W and (2 × 2)-OH-6W, since both represent important structural motives that are dominantly present on the Al_2O_3 wafers used in the experiments.[31]

Thermodynamic Analysis. The thermodynamically most favorable surface and adsorbate structure at given temperature and pressure conditions minimizes the Gibbs free surface energy $\Delta\gamma(T,p)$. The Gibbs free surface energy can be determined from DFT total energies by relating DFT formation energies E_{DFT}^{form} of different configurations to changes in the chemical potential $\Delta\mu_x$ of the adsorbed species,[32] where x = IPA, W, PA, and AA for isopropanol, water, methyl phosphonic

dx.doi.org/10.1021/am4008374 | ACS Appl. Mater. Interfaces 2013, 5, 6073−6080

acid and acetic acid, respectively. For our surface structures, $\Delta\gamma(T,p)$ is given by

$$\Delta\gamma(T,p) = \frac{1}{A}\left(E_{\mathrm{DFT}}^{\mathrm{form}} - \sum_x n_x \Delta\mu_x\right) \quad (2)$$

where $E_{\mathrm{DFT}}^{\mathrm{form}}$ is the difference in total energy of a specific surface configuration $E_{(2\times2)}^{\mathrm{slab}}(n_{\mathrm{Al_2O_3}}, n_x)$ and the sum of total energies of the relaxed water-free reference surface $E_{(1\times1)\text{-Al}}^{\mathrm{slab}}$ and the amount n_x of the various adsorbed molecules E_x^{mol}:

$$E_{\mathrm{DFT}}^{\mathrm{form}} = E_{(2\times2)}^{\mathrm{slab}}(n_{\mathrm{Al_2O_3}}, n_x) - \left(4E_{(1\times1)\text{-Al}}^{\mathrm{slab}} + n_{\mathrm{Al_2O_3}}E_{\mathrm{Al_2O_3}}^{\mathrm{bulk}} + \sum_x n_x E_x^{\mathrm{mol}}\right) \quad (3)$$

The term $n_{\mathrm{Al_2O_3}}E_{\mathrm{Al_2O_3}}^{\mathrm{bulk}}$ takes into account that we have to remove an appropriate number of Al_2O_3 units from water-free Al-terminated (1 × 1)-Al when the fully hydroxylated (2 × 2)-OH-6W surface is formed, with $E_{\mathrm{Al_2O_3}}^{\mathrm{bulk}}$ being the total energy of the bulk hexagonal unit cell per Al_2O_3 formula unit. Alternatively to the formation energy of a surface structure, it is also instructive to consider the adsorption energy of an individual molecule of species x on one of our two model surface structures. For the (2 × 2)-Al-4W and (2 × 2)-OH-6W surface, the adsorption energies are given by

$$E_{\text{Al-4W}}^{\mathrm{ad}} = E_{(2\times2)}^{\mathrm{slab}}(\Delta n_{\mathrm{W}}, n_x) - \left(E_{(2\times2)\text{-Al-4W}}^{\mathrm{slab}} + \Delta n_{\mathrm{W}}E_{\mathrm{W}}^{\mathrm{mol}} + n_x E_x^{\mathrm{mol}}\right) \quad (4)$$

and

$$E_{\text{OH-6W}}^{\mathrm{ad}} = E_{(2\times2)}^{\mathrm{slab}}(\Delta n_{\mathrm{W}}, n_x) - \left(E_{(2\times2)\text{-OH-6W}}^{\mathrm{slab}} + \Delta n_{\mathrm{W}}E_{\mathrm{W}}^{\mathrm{mol}} + n_x E_x^{\mathrm{mol}}\right) \quad (5)$$

respectively, where Δn_{W} is the change in the number of adsorbed water molecules compared to the initial model surface structure and n_x is always equal to one in the present study.

Phase diagrams describing the stability of different adsorbate structures are directly accessible from eq 2 by plotting $\Delta\gamma(T,p)$ as a function of $\Delta\mu_x$. In this study, we will only consider $\Delta\mu_x < 0$, since for positive values of $\Delta\mu_x$ it would become thermodynamically favorable to form condensates of species x on the surfaces. The chemical potentials $\Delta\mu_x$ can be related to temperature and pressure conditions in order to link the calculated phase diagrams to specific experimental environments. The temperature and pressure dependence of $\Delta\mu_x$ is tabulated in thermochemical tables.[33] The chemical potential of liquid water at ambient conditions is $\Delta\mu_{\mathrm{W}}$ (293 K,1 bar) = −0.57 eV.[34] Since we are especially interested in the stability of the SAMs under liquid water conditions, this value is indicated in the adsorption phase diagrams by a vertical line.

EXPERIMENTAL METHODS

In order to investigate the self-assembly of alkyl phosphonates and alkyl carboxylates on aluminum oxide surfaces, the static contact angle (SCA) of water on the SAM-terminated surfaces was measured as a function of immersion time in SAM solution. The substrates were fabricated by thermal evaporation of 30 nm aluminum on p-silicon substrates with a rate of 2.5 Å/s at pressures below $2\cdot10^{-6}$ mbar, followed by an oxygen plasma treatment at pressures of 0.2 mbar for 2 min (Diener Electronic Pico, 200 W) to yield an aluminum oxide layer (AlO_x) of approximately 3.6 nm thickness.[35] Subsequently, C_{17}−CA or C_{18}−PA were self-assembled from IPA solutions using concentrations of 1 mM for C_{17}−CA and 0.05 mM for C_{18}−PA. Long alkyl-chained molecules were chosen to generate a strong contrast in SCA measurements. Substrates were removed after specific times (between 1 min and 3 days), and the surfaces were gently rinsed with pure IPA and dried at 60 °C on a hot plate for 3 min. Static contact angles of H_2O were measured using a contact angle system OCA from Dataphysics in sessile drop mode with a drop volume of 2.0 μL. Desorption experiments were performed by immersing the SAM-decorated substrates in pure IPA and recording the SCA values as a function of immersion time. Exchange-reaction experiments were performed by immersing the SAM-decorated substrates in a solution of the molecule with the alternative anchor group in IPA for 3 days. In order to increase the difference in SCA values, we chose a solution of 0.05 mM partially fluorinated phosphonic acid 12,12,13,13,-14,14,15,15,16,16,17,17,18,18,18H-pentadecafluoro-octadecyl phosphonic acid ($F_{15}C_{18}$−PA) in place of C_{18}−PA.

COMPUTATIONAL RESULTS

Solvent Coverage. In the experiments, phosphonic and carboxylic acid are deposited from a solution of the acids in nominally dry IPA, so that the Al_2O_3 wafers only come into contact with moisture from the air and residual water in the solvent.[1,36] In a first step, we therefore tested whether IPA adsorbs on Al_2O_3 using calculations similar to those for the adsorption of water. From the results, we determined a two-dimensional phase diagram of the thermodynamic stability of adsorbed IPA on (2 × 2)-Al in the presence of water (see Figure 2).

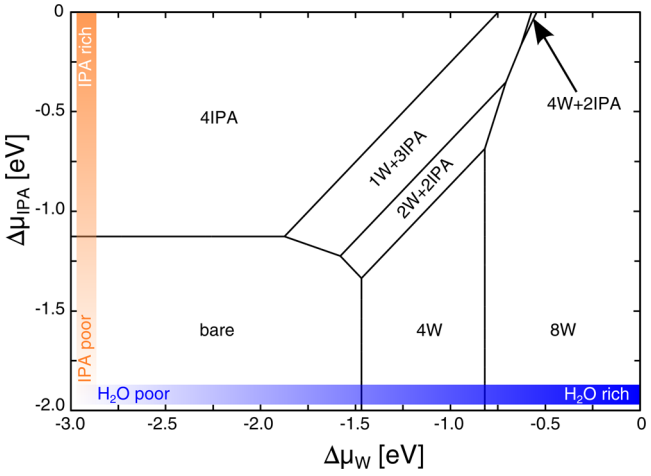

Figure 2. Surface phase diagram of mixed IPA and water (W) adsorption on (2 × 2)-Al.

The DFT calculations show that on the water-free (2 × 2)-Al surface IPA molecules adsorb and dissociate similarly to water but with a lower energy gain. As expected from the higher pK_a value (16.6 for IPA,[37] compared to 14.0 for water), IPA is able to displace all adsorbed and dissociated water molecules only at rather high IPA and low water chemical potentials. Mixed IPA/water phases are possible at intermediate chemical potentials; however, in the most important region describing liquid IPA/water conditions ($\Delta\mu > -1$ eV), water adsorption dominates.

To determine the IPA/water surface coverage to be expected under the conditions of the present experiments, we provide a rough estimate of the corresponding chemical potentials. $\Delta\mu_{\mathrm{W}}$ and $\Delta\mu_{\mathrm{IPA}}$ depend on temperature and the amount of water and IPA in the environment. For mixtures of substances, we can apply the formula $\Delta\mu_x = \Delta\mu_x^{\mathrm{ref}} + k_{\mathrm{B}}T\ln(a_x)$, where a_x is the activity of substance x. Commercially available IPA contains residual water in the range of 0.003 vol % up to 0.5 vol %.[38,39] When working with anhydrous IPA, Raoult's Law can be applied for the activity coefficient of IPA ($\gamma_{\mathrm{IPA}} = 1$), and the activity of IPA is equal to its amount fraction. The activity coefficient of water in IPA is available from experimental data[40] down to a water amount fraction of $x_{\mathrm{W}} = 0.1505$. We extrapolated the water activity coefficient to a residual water

content of 0.003 vol %, which gave $\gamma_W^{0.003}$ = 4.0846. This shifts $\Delta\mu_W$ with respect to the value of liquid water (at ambient conditions) by −0.19 eV, so that the chemical potential of water in the present experiments is in the order of $\Delta\mu_W^{0.003}$ = −0.76 eV.

To estimate the chemical potential of pure liquid IPA, we consider IPA to have a similar but weaker reactivity toward the surface than water. We consider this change in reactivity to be reasonably covered by the different pK_a values of the substances, so we take the $\Delta\mu_W$ value for liquid water times the fraction of the pK_a values of IPA and water and estimate the chemical potential of IPA to be about $\Delta\mu_{IPA}$ = −0.66 eV.

At these chemical potentials, we are very close to the phase boundaries where the surface coverage changes from two to one adsorbed molecule per surface unit cell and where IPA starts to displace water from the surface (see Figure 2). For simplicity, we neglected in the calculations a possible exchange of water by IPA, and the low humidity conditions in the experiment led us to choose the (2 × 2)-Al-4W configuration for our study of PA and AA adsorption. However, it should be kept in mind that structures with water substituted by IPA might have a similar thermodynamic stability. Furthermore, in the course of our adsorption studies, the stability of higher water coverage was frequently probed (see Supporting Information).

Adsorption of Phosphonic Acid (PA) on (2 × 2)-Al. The (2 × 2)-Al-4W surface provides four identical binding sites for PA, which can therefore bind in a monodentate (m), bidentate (b), or tridentate (t) manner to the surface. In addition, interactions between PA and the surface via hydrogen bonds before or after covalent bond formation are possible. While mono- and bidentate bonds to the surface are formed by recombination of a water molecule via protonation of a surface OH group by PA (see Figure 3a), the third bond in the tridentate binding mode is found to be formed when a dissociated water molecule reassembles in order to provide an empty adsorption site for the oxygen atom from the PA molecule (see Figure 3b). We have investigated all three types of PA bonding. Several orientations of the PA molecules and possible hydrogen bonds as well as different amounts of adsorbed water were taken into account (see Supporting Information). Hydrogen bonding to the surface was not defined explicitly but is an inherent part of the interactions between acid and surface.

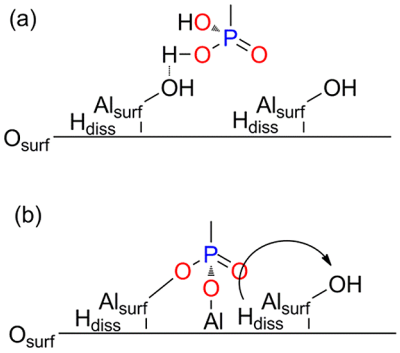

Figure 3. Schematic view of PA bonding to hydroxylated Al_2O_3 surfaces. (a) Monodentate PA bonds are formed by recombination of a surface hydroxyl group with an acidic PA proton and elimination of a water molecule. Similarly, bidentate PA bonding occurs via elimination of a second water molecule. (b) After transfer of an H_{diss} to a surface hydroxyl group and release of a third water molecule, PA can bind in a tridentate fashion.

In the following, we report only those structures that appear as thermodynamically stable configurations in the surface phase diagrams (see Table 1 and Figure 4). Configurations are labeled according to their water content and PA binding mode (subscript). Figure 4 shows that the configuration (2 × 2)-Al-3W-1PA$_m$ with monodentate PA bonding to the surface after removing one adsorbed water molecule is most stable over a broad range of $\Delta\mu_W$. At higher water chemical potential, the formation of the bidentate (2 × 2)-Al-4W-1PA$_b$ is preferred. This is the most stable structure if the system is exposed to liquid water at ambient conditions, as indicated by the vertical

Table 1. Formation and Adsorption Energies (in eV) of Stable PA and AA Configurations on (2 × 2)-Al-4W

configuration	E_{DFT}^{form}	E_{Al-4W}^{ad}
(2 × 2)-Al-3W-1PA$_m$	−6.95	−1.08
(2 × 2)-Al-4W-1PA$_b$	−7.57	−1.69
(2 × 2)-Al-3W-1AA$_m$	−6.10	−0.23
(2 × 2)-Al-4W	−5.87	0

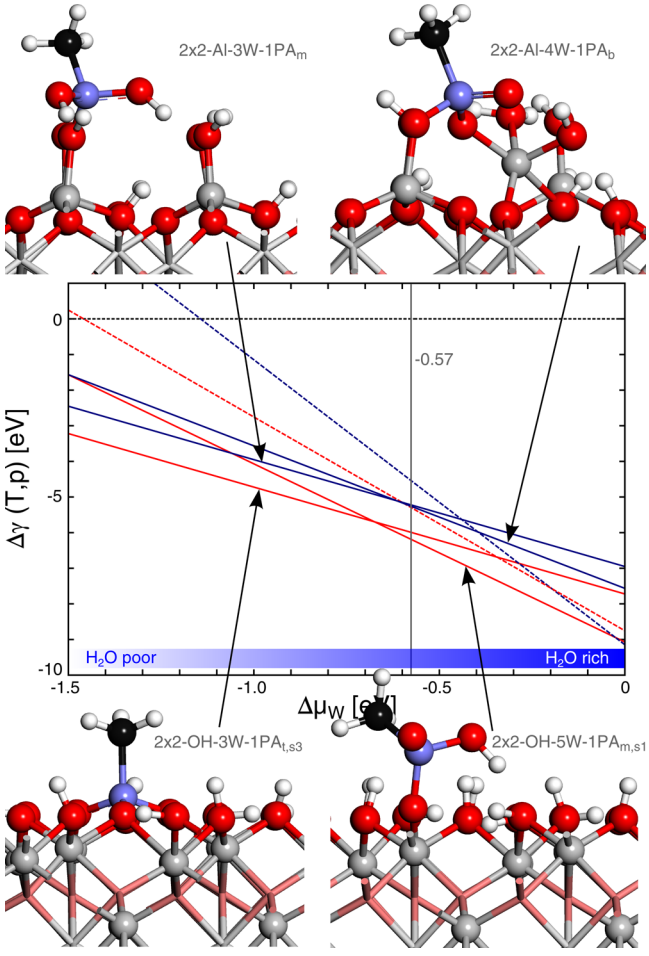

Figure 4. Surface phase diagram for PA adsorption. Top: The two most stable configurations of PA on (2 × 2)-Al are (2 × 2)-Al-3W-1PA$_m$ and (2 × 2)-Al-4W-1PA$_b$. Bottom: The two most stable configurations of PA on (2 × 2)-OH are (2 × 2)-OH-3W-1PA$_{t,s3}$ and (2 × 2)-OH-5W-1PA$_{m,s1}$. The horizontal dashed line denotes (2 × 2)-Al; the sloped dashed lines denote (2 × 2)-Al-8W and (2 × 2)-OH-6W, respectively.

dx.doi.org/10.1021/am4008374 | ACS Appl. Mater. Interfaces 2013, 5, 6073−6080

gray line at −0.57 eV in Figure 4. This means that single PA molecules on these surfaces in the (2 × 2)-Al-4W-1PA$_b$ configuration cannot be removed by water.

Adsorption of phosphonic acid (PA) on (2 × 2)-OH. The fully hydroxylated (2 × 2)-OH-6W surface exhibits three different binding sites s_1, s_2, and s_3 (see Figure 1b) that differ in the distance of the first subsurface Al atom from the top OH layer and in the tripodal orientation of the OH groups around the Al atom.[29] This leads to different energies for bi- or tridentate linkages at the three sites, while the binding energy for the monodentate adsorption is essentially independent of the type of site (see Table 2 and Supporting Information). The

Table 2. Formation and Adsorption Energies (in eV) of Stable PA and AA Configurations on (2 × 2)-OH-6W

configuration	E_{DFT}^{form}	E_{OH-6W}^{ad}
(2 × 2)-OH-5W-1PA$_{m,s1}$	−9.05	−0.30
(2 × 2)-OH-5W-1PA$_{m,s2}$	−9.01	−0.26
(2 × 2)-OH-5W-1PA$_{m,s3}$	−9.07	−0.32
(2 × 2)-OH-3W-1PA$_{t,s3}$	−7.72	1.03
(2 × 2)-OH-5W-1AA$_{m,s1}$	−8.33	0.43
(2 × 2)-OH-5W-1AA$_{m,s2}$	−8.57	0.19
(2 × 2)-OH-5W-1AA$_{m,s3}$	−8.44	0.31
(2 × 2)-OH-6W	−8.75	0

phase diagram (see Figure 4) shows that tridentate coordination is accessible only on s_3 at low water chemical potentials, while the mono- and bidentate coordination patterns are the only means of binding to s_1 or s_2. Monodentate coordination is the most stable configuration on s_1 and s_2 over a broad range of experimentally accessible $\Delta\mu_W$. Apart from the shift from tri- to monodentate linkage on s_3, changes in the water chemical potential do not affect bonding of PA on (2 × 2)-OH-6W. Monodentate coordination of PA on the surface is stable in liquid water under standard conditions.

The PA molecules arrange on the surfaces in ways that resemble the corresponding crystal structure of aluminum oxide, i.e., the oxygen atoms of the anchor groups move to sites that would be occupied by oxygen atoms in the Al_2O_3 bulk. The deviations from these positions are small, and especially on the OH-terminated surface, PA molecules fit perfectly into the terminating surface layer, which accounts for the high stability of PA on this type of surface.

The combined phase diagram for (2 × 2)-Al and (2 × 2)-OH (see Figure 4) gives insight into the change of PA bonding on the different surface types under varying conditions. Bonding depends on the humidity of the environment. On (2 × 2)-Al surfaces, the dominant monodentate bonding changes to bidentate bonding for higher $\Delta\mu_W$. On (2 × 2)-OH surfaces, PA is expected to bind to all three binding sites $s_{1,2,3}$ in a monodentate manner for a large range of $\Delta\mu_W$, but is capable of binding to s_3 in a tridentate manner if $\Delta\mu_W$ is lowered. This result shows the importance of thermodynamic analysis for understanding and predicting bonding configurations: From the pure DFT values in Table 2, tridentate bonding would not be a stable configuration. Only the phase diagram makes it clear that a change from monodentate to tridentate bonding is favorable under experimental accessible conditions, i.e., anhydrous IPA as solvent. Considering that both surface models could be present on the AlO_x layers used in the experiment, it becomes clear why it is so hard to give definite statements on the bonding of phosphonic acids by experiments.[41,42] Different bonding types are stable on the different surfaces under the same experimental conditions, and they strongly depend on the amount of water in the environment.

Adsorption of Acetic Acid (AA) on (2 × 2)-Al. In contrast to PA, AA can only bind in mono- or bidentate fashion to the surface. While monodentate coordination is possible by etching a surface hydroxyl group (see Figure 5a), again reassembly of a dissociated water molecule by mediation of the carboxyl oxygen is needed for bidentate linkage (see Figure 5b).

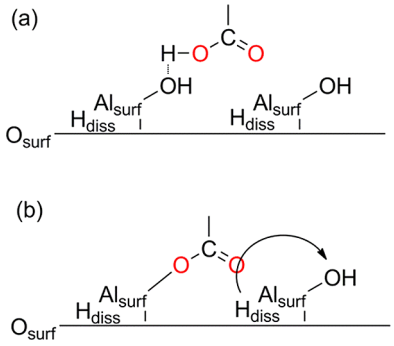

Figure 5. Schematic view of AA bonding to hydroxylated Al_2O_3 surfaces. (a) Monodentate AA bonds are formed by recombination of a surface hydroxyl group with an acidic AA proton and elimination of a water molecule. (b) After transfer of an H_{diss} to a surface hydroxyl group and release of a second water molecule, AA can bind in a bidentate fashion.

In general, the adsorption energy for AA on (2 × 2)-Al-4W is significantly lower than for PA (see Table 1 and Supporting Information). The difference in the adsorption energies between AA and PA for monodente bonding shows that AA is generally less stable toward water and that the back reaction of dissolution and hydroxylation of the binding site requires a smaller shift of the chemical potential. This is expected from the higher pK_a of AA (4.77[43]) compared to PA (2.41 for $RPO(OH)_2$ and 7.54 for RPO_2OH).[44] The calculated phase diagram (see Figure 6) shows that monodentate coordination is the only stable configuration for binding on (2 × 2)-Al under the experimental conditions. In contrast to PA, AA is detached from the surface at higher water chemical potential. AA does not form stable layers in liquid water at ambient conditions and thus can be easily washed off the (2 × 2)-Al surface.

Adsorption of Acetic Acid (AA) on (2 × 2)-OH. AA prefers monodentate coordination to the (2 × 2)-OH-6W surface over the full range of the water chemical potential. The three different binding sites give very similar binding energies for monodentate coordination (see Supporting Information). During geometry optimization, s_2-bound AA shifted the bond from Al_{s2} to Al_{s1} as the s_2-binding carboxyl oxygen is close to the neighboring Al_{s1}. This might result in slightly less repulsion from the other oxygen and more flexibility in H-bond formation. Apart from this bond change, AA remained close to the s_2 configuration, which is more important than the specific $Al_{s1,2}$ site to which AA binds, as it is in the nature of the surface oxygen atoms of (2 × 2)-OH to bridge between the topmost Al atoms, i.e., Al_{s1} and Al_{s2}, and changes in AA position of only 0.3 Å change the site of the bond. One should consider here that both Al_{s1} and Al_{s2} are only partially coordinated due to the etching of surface hydroxyl by AA prior to bonding.

dx.doi.org/10.1021/am4008374 | ACS Appl. Mater. Interfaces 2013, 5, 6073−6080

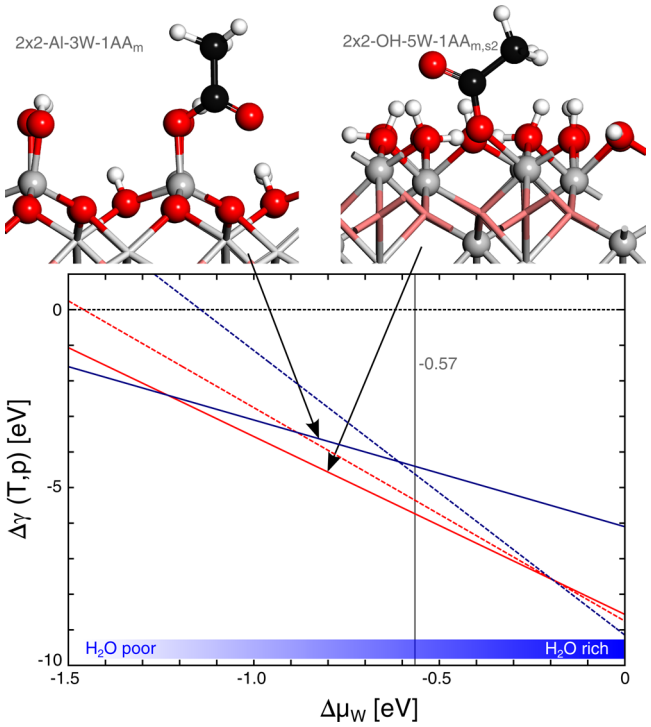

Figure 6. Surface phase diagram for AA adsorption. (2 × 2)-Al-3W-1AA$_m$ is the most stable configuration of AA on (2 × 2)-Al, and (2 × 2)-OH-5W-1AA$_{m,s2}$ is the preferred binding mode of AA on (2 × 2)-OH. The horizontal dashed line denotes (2 × 2)-Al; the sloped dashed lines denote (2 × 2)-Al-8W and (2 × 2)-OH-6W, respectively.

The prospective bidentate coordination of AA is not observed in the calculations. For all three binding sites, structural relaxations starting from bidentate coordination geometries ended as carbonate-like structures (see Figure 7)

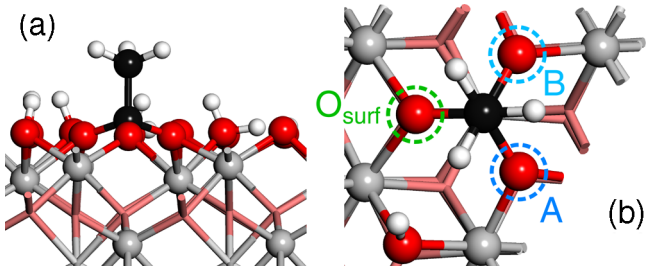

Figure 7. Carbonate-like structure of adsorbed AA on (2 × 2)-OH-6W. (a) Side view and (b) top view showing the first (A) and second (B) binding site of AA. O$_{surf}$ denotes a deprotonated surface hydroxyl group.

with deprotonated surface oxygen (denoted O$_{surf}$ in Figure 7). Deprotonated surface oxygen is available because a proton from the nearby surface hydroxyl group containing O$_{surf}$ was transferred to the hydroxyl group at site B. Water is released (see Figure 5b), and a second binding site becomes available (denoted as B in Figure 7). The detailed phase diagram for the adsorption of AA on AlO$_x$ (see Figure S5 in the Supporting Information) suggests that the carbonate-like structures can only form for very low $\Delta\mu_W$ and therefore should not play a role under standard experimental conditions. In contrast to the results obtained on (2 × 2)-Al, monodentatedly coordinated AA is found to be stable toward liquid water on (2 × 2)-OH-6W on all three binding sites.

The combined phase diagram for the two aluminum oxide surfaces (see Figure 6) shows the overall higher stability of monodentatedly coordinated AA on (2 × 2)-OH-6W compared to adsorption on (2 × 2)-Al. As with PA, oxygen from AA anchor groups integrate into the hydroxyl layer on (2 × 2)-OH. On (2 × 2)-Al, the bond to the surface is perpendicular to the surface plane and the remaining carboxyl oxygen forms a hydrogen bond to H$_{diss}$ instead to a neighboring hydroxyl group. This is due to the shorter length of the CO bond in AA (1.25 Å) compared to PO bonds in PA (1.50 Å) and the shorter bond length of AA to the surface (1.34 Å, compared to 1.58 Å for PA), which prevents the formation of hydrogen bonds to hydroxyl groups. The lower binding energy of AA compared to PA on both surfaces (see Tables 1 and 2) shows that, in a competing situation between both acids, binding of PA would be favored over AA and that exchange of carboxylates with phosphonates is thermodynamically possible.

EXPERIMENTAL RESULTS

Adsorption on AlO$_x$ Surfaces. In order to confirm the theoretical results from the phase diagram calculations, we have investigated the adsorption of IPA, C$_{18}$−PA, and C$_{17}$−CA on AlO$_x$ surfaces created by O$_2$ plasma treatment directly from thermally evaporated Al layers. The morphology of converted or deposited AlO$_x$ layers is amorphous compared to α-Al$_2$O$_3$ but provides on average comparable binding sites and represents the practical surfaces used in devices.[1,6,10] The average surface roughness of rms = 1.00 nm was determined by AFM measurements on a 10 μm × 10 μm area. The adsorption to self-assembled monolayers of those molecules can be tracked easily by measuring the static contact angle (SCA) of water, which relies on a difference between the SCA values of the starting surface and the SAM. However, several other methods have been used in the past to prove the validity of the SCA measurements, e.g., XPS, AFM, SFG, and electric data from devices.[1,13,15,17,34] Typically, a plasma-generated AlO$_x$ that has been exposed to ambient air (terminated with OH-groups) exhibits an SCA value of <20° (Figure 8c) because of the high surface energy of >50 mN/m.[12] After storing the surface in IPA for 1 day, the SCA value increases to 39°, indicating coverage by the more hydrophobic alcohol (Figure 8d). The time-dependent adsorption of C$_{18}$−PA and C$_{17}$−CA is shown in Figure 8a. The adsorption follows a typical Langmuir isotherm to saturation to a densely packed monolayer in both cases. The similar *n*-alkyl chain compositions of C$_{18}$−PA and C$_{17}$−CA mean that the SCA values are very similar after 4320 min (3 days) with 108° (Figure 8f) and 105° (Figure 8e), respectively. However, while the C$_{18}$−PA saturates within 15 min, the increase in SCA value of C$_{17}$−CA is much slower and saturation occurs only after 3 days. The effect is even stronger considering that the concentration of C$_{17}$−CA is 200 times larger than that of C$_{18}$−PA.

This clearly indicates that the adsorption of phosphonates is faster than that of carboxylates with comparable molecular structure. These results also show that a weakly interacting molecule (e.g., IPA) can easily be exchanged by a stronger binder (PA or CA), even when available in large excess (IPA as solvent).

Desorption. The self-assembly of molecular monolayers on surfaces in solution can be described as an interplay of adsorbed and desorbed molecules in which the densely packed SAM

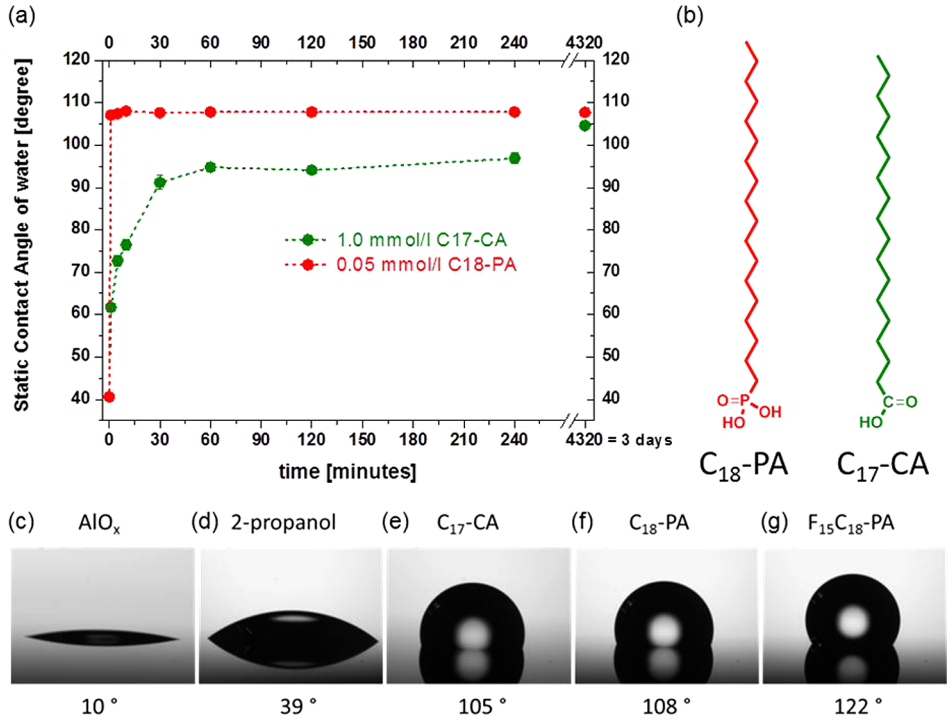

Figure 8. (a) Time-dependent adsorption behavior of *n*-octadecylphosphonic acid (C_{18}–PA) and stearic acid (C_{17}–CA) on an AlO_x surface monitored by static contact angle measurements. (b) Chemical structure of C_{18}–PA (red) and C_{17}–CA (green). (c–g) Wetting behavior of water on AlO_x surface terminated with OH, isopropanol, and SAMs.

represents the equilibrium state. The stability of a SAM in a pure solvent (without solute C_{17}–CA or C_{18}–PA) can disturb this equilibrium, and desorption could become a significant process. The qualitative difference of desorption of two comparable molecules with different anchor groups allows conclusions about the binding strength. The SAMs of C_{18}–PA and C_{17}–CA on AlO_x surfaces were stored for 150 h in pure IPA. The SCA value of the substrate with C_{18}–PA remained virtually constant at 108°, but that of the C_{17}–CA sample decreased to 61% of the initial value, indicating that phosphonates bind faster and stronger than carboxylates.

Exchange. In order to investigate the exchange of adsorbed carboxylates by phosphonates by SCA measurements, we used a phosphonate of comparable chain length but with a partially fluorinated alkyl chain ($F_{15}C_{18}$–PA). SAMs of $F_{15}C_{18}$–PA exhibit even lower surface energy (9.3 mN/m) than C_{18}–PA (20 mN/m) and have a larger SCA value of 122°. Exchange experiments show that, after storing the C_{17}–CA coated sample in a 0.05 mM solution of $F_{15}C_{18}$–PA in IPA, the SCA value increased from 106° to 122°. The cross experiment ($F_{15}C_{18}$–PA SAM in a C_{17}–CA solution) does not lead to a change in the SCA value of 122°. This indicates that phosphonates can exchange carboxylates but not vice versa.

CONCLUSIONS

Bonding energies and geometries of acetic acid and methyl phosphonic acid on an Al-terminated and an OH-terminated $Al_2O_3(0001)$ surface were investigated by DFT calculations and thermodynamic analysis. Calculations were accompanied by experiments to confirm the results. AA and PA served as models for stearic acid and *n*-octadecylphosphonic acid, respectively, which were used experimentally to prepare SAMs on AlO_x. The use of two different surface models was deemed necessary as the specific structure of the AlO_x films in the experiments is not well-defined. While the Al-terminated surface may be present due to the manufacturing process, the OH-terminated surface is thermodynamically more stable.

PA is predicted to bind more strongly to either surface than AA: on (2 × 2)-Al surfaces in a monodentate fashion or on (2 × 2)-OH surfaces in a mono- or tridentate manner depending on $\Delta\mu_W$. AA is predicted to bind to either surface type in a monodentate manner. While PA is predicted to be generally stable against water on both surfaces, AA is stable only on (2 × 2)-OH. Both the different binding of PA on (2 × 2)-OH and the adsorption of AA emphasize the necessity of thermodynamic analysis. Both the bond change and the stability of adsorbed AA would not be clear from DFT results alone.

SCA measurements show a successful coating of AlO_x with IPA, C_{17}–CA, or C_{18}–PA. A change in the contact angle for IPA may indicate (2 × 2)-Al type areas as mixed phases are predicted by the calculations. On the other hand, partial desorption of C_{17}–CA from a coated sample could equally be an indication for (2 × 2)-OH type areas. Exchange of C_{17}–CA by C_{18}–PA is suggested by the calculations and was confirmed by the experiments.

ASSOCIATED CONTENT

Supporting Information

Additional adsorption phase diagrams and detailed tables of DFT total energies. This material is available free of charge via the Internet at http://pubs.acs.org.

AUTHOR INFORMATION

Corresponding Author

*E-mail: Tim.Clark@chemie.uni-erlangen.de.

Notes

The authors declare no competing financial interest.

■ ACKNOWLEDGMENTS

This work was supported by the Cluster of Excellence "Engineering of Advanced Materials" (EAM) financed by Deutsche Forschungsgemeinschaft (DFG). We thank the Regionales Rechenzentrum Erlangen (RRZE) for computer time on its LiMa high-performance cluster.

■ REFERENCES

(1) Klauk, H.; Zschieschang, U.; Pflaum, J.; Halik, M. *Nature* **2007**, *445*, 745−748.
(2) Halik, M.; Klauk, H.; Zschieschang, U.; Schmid, G.; Dehm, C.; Schutz, M.; Maisch, S.; Effenberger, F.; Brunnbauer, M.; Stellacci, F. *Nature* **2004**, *431*, 963−966.
(3) Klauk, H. *Chem. Soc. Rev.* **2010**, *39*, 2643−2666.
(4) Sekitani, T.; Zschieschang, U.; Klauk, H.; Someya, T. *Nat. Mater.* **2010**, *9*, 1015−1022.
(5) Sekitani, T.; Yokota, T.; Zschieschang, U.; Klauk, H.; Bauer, S.; Takeuchi, K.; Takamiya, M.; Sakurai, T.; Someya, T. *Science* **2009**, *326*, 1516−1519.
(6) Halik, M.; Hirsch, A. *Adv. Mater.* **2011**, *23*, 2689−2695.
(7) Zschieschang, U.; Halik, M.; Klauk, H. *Langmuir* **2008**, *24*, 1665−1669.
(8) Smits, E. C. P.; Mathijssen, S. G. J.; van Hal, P. A.; Setayesh, S.; Geuns, T. C. T.; Mutsaers, K. A. H. A.; Cantatore, E.; Wondergem, H. J.; Werzer, O.; Resel, R.; Kemerink, M.; Kirchmeyer, S.; Muzafarov, A. M.; Ponomarenko, S. A.; de Boer, B.; Blom, P. W. M.; de Leeuw, D. M. *Nature* **2008**, *455*, 956−959.
(9) Mathijssen, S. G.; Smits, E. C.; van Hal, P. A.; Wondergem, H. J.; Ponomarenko, S. A.; Moser, A.; Resel, R.; Bobbert, P. A.; Kemerink, M.; Janssen, R. A.; de Leeuw, D. M. *Nat. Nanotechnol.* **2009**, *4*, 674−680.
(10) Novak, M.; Ebel, A.; Meyer-Friedrichsen, T.; Jedaa, A.; Vieweg, B. F.; Yang, G.; Voitchovsky, K.; Stellacci, F.; Spiecker, E.; Hirsch, A.; Halik, M. *Nano Lett.* **2011**, *11*, 156−159.
(11) Zschieschang, U.; Ante, F.; Schlorholz, M.; Schmidt, M.; Kern, K.; Klauk, H. *Adv. Mater.* **2010**, *22*, 4489−4493.
(12) Amin, A. Y.; Reuter, K.; Meyer-Friedrichsen, T.; Halik, M. *Langmuir* **2011**, *27*, 15340−15344.
(13) Rumpel, A.; Novak, M.; Walter, J.; Braunschweig, B.; Halik, M.; Peukert, W. *Langmuir* **2011**, *27*, 15016−15023.
(14) Jedaa, A.; Salinas, M.; Jäger, C. M.; Clark, T.; Ebel, A.; Hirsch, A.; Halik, M. *Appl. Phys. Lett.* **2012**, *100*, 063302.
(15) Burkhardt, M.; Jedaa, A.; Novak, M.; Ebel, A.; Voitchovsky, K.; Stellacci, F.; Hirsch, A.; Halik, M. *Adv. Mater.* **2010**, *22*, 2525−2528.
(16) Hotchkiss, P. J.; Jones, S. C.; Paniagua, S. A.; Sharma, A.; Kippelen, B.; Armstrong, N. R.; Marder, S. R. *Acc. Chem. Res.* **2012**, *45*, 337−346.
(17) Lenz, T.; Schmaltz, T.; Novak, M.; Halik, M. *Langmuir* **2012**, *28*, 13900−13904.
(18) Perdew, J. P.; Burke, K.; Ernzerhof, M. *Phys. Rev. Lett.* **1996**, *77*, 3865−3868.
(19) Vanderbilt, D. *Phys. Rev. B* **1990**, *41*, 7892−7895.
(20) Giannozzi, P.; Baroni, S.; Bonini, N.; Calandra, M.; Car, R.; Cavazzoni, C.; Ceresoli, D.; Chiarotti, G. L.; Cococcioni, M.; Dabo, I.; Dal Corso, A.; de Gironcoli, S.; Fabris, S.; Fratesi, G.; Gebauer, R.; Gerstmann, U.; Gougoussis, C.; Kokalj, A.; Lazzeri, M.; Martin-Samos, L.; Marzari, N.; Mauri, F.; Mazzarello, R.; Paolini, S.; Pasquarello, A.; Paulatto, L.; Sbraccia, C.; Scandolo, S.; Sclauzero, G.; Seitsonen, A. P.; Smogunov, A.; Umari, P.; Wentzcovitch, R. M. *J. Phys.: Condens. Matter* **2009**, *21*, 395502.
(21) Prokof'ev, V. Y.; Gordina, N. E.; Zhidkova, A. B.; Efremov, A. M. *J. Mater. Sci.* **2012**, *47*, 5385−5392.
(22) Barth, C.; Reichling, M. *Nature* **2001**, *414*, 54−57.
(23) Wang, X.-G.; Chaka, A.; Scheffler, M. *Phys. Rev. Lett.* **2000**, *84*, 3650−3653.
(24) Mason, S. E.; Iceman, C. R.; Trainor, T. P.; Chaka, A. M. *Phys. Rev. B* **2010**, *81*, 125423.
(25) Hass, K. C.; Schneider, W. F.; Curioni, A.; Andreoni, W. *Science* **1998**, *282*, 265.
(26) Ruberto, C.; Yourdshahyan, Y.; Lundqvist, B. *Phys. Rev. B* **2003**, *67*, 195412.
(27) Chaplin, M. F. Water's hydrogen bond strength. In *Water and Life: The unique properties of H2O*, 1st ed.; Lynden-Bell, R. M., Conway Morris, S., Barrow, J. D., Finney, J. L., Harper, C. L., Eds.; CRC Press: Boca Raton, 2010; pp 69−86.
(28) Thissen, P.; Grundmeier, G. *Phys. Rev. B* **2009**, *80*, 245403.
(29) Luschtinetz, R.; Oliveira, A. F.; Frenzel, J.; Joswig, J.-O.; Seifert, G.; Duarte, H. A. *Surf. Sci.* **2008**, *602*, 1347−1359.
(30) Luschtinetz, R.; Oliveira, A. F.; Duarte, H. A.; Seifert, G. *Z. Anorg. Allg. Chem.* **2010**, *636*, 1506−1512.
(31) Novak, M.; Jäger, C. M.; Rumpel, A.; Kropp, H.; Peukert, W.; Clark, T.; Halik, M. *Org. Electron.* **2010**, *11*, 1476−1482.
(32) Qian, G.-X.; Martin, R.; Chadi, D. *Phys. Rev. B* **1988**, *38*, 7649−7663.
(33) National Institute of Standards and Technology. NIST-JANAF Thermochemical Tables. http://kinetics.nist.gov/janaf/html/H-064.html (accessed 6th May 2013).
(34) Klaumünzer, M.; Mačković, M.; Ferstl, P.; Voigt, M.; Spiecker, E.; Meyer, B.; Peukert, W. *J. Phys. Chem. C* **2012**, *116*, 24529−24537.
(35) Novak, M.; Schmaltz, T.; Faber, H.; Halik, M. *Appl. Phys. Lett.* **2011**, *98*, 093302.
(36) Jedaa, A.; Burkhardt, M.; Zschieschang, U.; Klauk, H.; Habich, D.; Schmid, G.; Halik, M. *Org. Electron.* **2009**, *10*, 1442−1447.
(37) Nakagawa, Y.; Uehara, K.; Mizuno, N. *Inorg. Chem.* **2005**, *44*, 9068−9075.
(38) Sigma Aldrich. 2-Propanol, anhydrous, 99.5%. http://www.sigmaaldrich.com/catalog/product/sial/278475?lang=de&region=DE (accessed 6th May 2013).
(39) Sigma Aldrich. 2-Propanol, Laboratory Reagent, ≥99.5% http://www.sigmaaldrich.com/catalog/product/sial/109827?lang=de&region=DE (accessed 6th May 2013).
(40) Khalfaoui, B.; Meniai, A. H.; Borja, R. *Fluid Phase Equilib.* **1997**, *127*, 181−190.
(41) Thissen, P.; Valtiner, M.; Grundmeier, G. *Langmuir* **2010**, *26*, 156−164.
(42) Levine, I.; Weber, S. M.; Feldman, Y.; Bendikov, T.; Cohen, H.; Cahen, D.; Vilan, A. *Langmuir* **2012**, *28*, 404−415.
(43) Haynes, W. M., Ed. *CRC Handbook of Chemistry and Physics*, 93rd ed., 2012−2013 [Online]; Taylor and Francis Group; http://www.hbcpnetbase.com (accessed 6th May 2013).
(44) Abbott, A.; Sierakowski, T.; Kiddle, J. J.; Clark, K. K.; Mezyk, S. P. *J. Phys. Chem. B* **2010**, *114*, 7681−7685.